Analyzing Wireless Networks using Binomial Line Cox Processes

[†]Mohammad Taha Shah, *Graduate Student Member, IEEE*, [†]Gourab Ghatak, *Member, IEEE*,
[+]Souradip Sanyal, and [‡]Martin Haenggi, *Fellow, IEEE*
[†]Indian Institute of Technology Delhi, New Delhi, 110016 India; [+]Department of ECE, IIIT-Delhi, Delhi 110020
[‡]Department of Electrical Engineering, University of Notre Dame, Notre Dame, IN 46556 USA
Email:bsz218183@iitd.ac.in, gghatak@ee.iitd.ac.in, souradip20156@iiitd.ac.in, and mhaenggi@nd.edu

***Abstract*—The stochastic geometry analysis of vehicular networks and on-street deployment of base stations is largely based on Cox processes driven by Poissonian models. In this paper, we investigate scenarios where a model with a finite and deterministic number of streets, termed the binomial line process (BLP), is more accurate. We characterize the statistical properties of the BLP and the corresponding binomial line Cox process (BLCP). We derive the line length density and the intersection density for the BLP and demonstrate how it models the inhomogeneity of the streets in a city. Finally, leveraging the derived framework, we analyze the performance of a network whose access points are deployed along the streets of a city. Our study captures the variation in the service performance of the users across different locations of a city and thus it leads to key network planning and dimensioning rules for the operators.**

***Index Terms*—Stochastic geometry, Line processes, Cox process, Wireless communications**

I. Introduction

Stochastic geometry lends key tools for the mathematical analysis of wireless cellular and ad hoc networks [3]–[5]. Recently, Poissonian line models in stochastic geometry have been applied in characterizing the streets of cities in order to study cellular and vehicular networks [6], [7]. In this paper, we develop and present a novel stochastic geometry tool for the modeling and analysis of vehicular networks. In particular, we introduce the binomial line process (BLP) to model the streets of a city and a corresponding Cox process to emulate the locations of wireless access points (APs) and vehicles.

Recall that line processes are spatial stochastic processes used for studying urban planning, river network modeling, wireless communication, and industrial automation [3], [8]. Based on line processes we can study line-driven Cox processes that help to model the locations of points on the line processes. In wireless networks, such models are employed to emulate the locations of APs deployed along the streets of a city, e.g., see [9] and [10]. The signal coverage of any point in the network for such on-street deployed small cells is of significant interest for the network operators and is the focus of this work.

A. Related Work

In literature, several line processes have been proposed and characterized, including the Poisson line process (PLP), the Poisson Voronoi tessellation (PVT), and the Poisson lilypond model [11]–[14]. The PLP [7], [13] is the most popular choice for modeling wireless networks due to its remarkable tractability. We refer the reader to the works by Chetlur *et al.* [15], [16] for a detailed discussion on the PLP model and its application in analyzing wireless networks. However, the PLP does not accurately account for finite street lengths, T-junctions, and varying street densities across cities. Recently, Jeyaraj *et al.* [13] proposed a Cox model framework that improved the accuracy of line process models by considering T-junctions, stick processes, and Poisson lilypond models. However, the authors did not take into account the variable street densities within a single city. In this regard, the authors in [17] used multi-density PVT and PLP to emulate the streets of Lyon, wherein, the parameters for the PVT are manually adjusted to match the street structures in various parts of the city. On the contrary, this paper focuses on studying non-homogeneous line processes to better model the characteristics of urban scenarios i.e., the streets near the city center are typically denser than those in the suburbs. In this paper, we introduce a new stochastic line process that can replicate the distinct street structures in both the city center and the suburbs using a fixed set of parameters. Furthermore, the city administrations construct streets on a case-by-case basis, so a deterministic number of streets usually characterizes the street network of a city. To address this, we recently have introduced the BLP [18], which consists of a fixed number of lines generated i.e. n_{B} within a bounded set. The BLP can capture the varying street and street length densities within a single city, making it useful for contrasting the performance of downtown and suburban users. In comparison, PLP models are stationary and restricted to a single fixed density.

B. Contributions

In this paper, we characterize the newly introduced BLP and binomial line Cox process (BLCP) models. In particular, we derive the line length and intersection measures and the respective densities. Then, the probability generating functional (PGFL) of the BLCP is derived, and based on it, we analyze the success probability of wireless networks where the locations of the APs form a BLCP. Our analysis captures the difference in the performance experienced by a city-center user to that of a suburban user and thus highlights the efficacy of the model.

The codes for generating the numerical results of this paper are available for download [1]. An extended version of the paper can be found in [2] and it also has been submitted for a possible journal publication.

II. Preliminaries

A. Binomial Line Process (BLP)

A BLP $\mathcal{L}$ is a finite collection of lines in the two-dimensional Euclidean plane $\mathbb{R}^2$ generated within a distance R from the origin. Formally,

$$\mathcal{L} \subset Q \triangleq \bigcup_{r\in\mathbb{R}\cap[-R,R],\theta\in[0,\pi)} \big\{(x,y)\in\mathbb{R}^2 : x\cos\theta + y\sin\theta = r\big\}. \tag{1}$$

Thus, a BLP consists of lines that correspond to the points of a binomial point process (BPP) defined on the finite cylinder $\mathcal{D} := [0,\pi)\times[-R,R]$, called the generating set of $\mathcal{L}$. The BLP is non-stationary by construction, and its properties depend on the distance from the origin rather than orientation. We consider a test point at $(0, r_0)$. The void probability of the BLP from the perspective of this point, and consequently, the distance distribution to the nearest line from this point is given in the following result.

Theorem 1. [18] *The probability that no line of the BLP intersects with $\mathcal{B}((0,r_0),t)$ is*

$$\mathcal{V}_{\mathrm{BLP}}(n_{\mathrm{B}},\mathcal{B}((0,r_0),t)) = \left(\frac{2\pi R - A_{\mathrm{D}}(r_0,t)}{2\pi R}\right)^{n_{\mathrm{B}}},$$

where, n_{B} is the number of lines of $\mathcal{L}$ and $A_{\mathrm{D}}(r_0,t)$, the area of the so-called domain band is evaluated as

$$A_{\mathrm{D}}(r_0,t) = \begin{cases} 2\pi t; & \text{for } r_0+t\le R \\ 2\pi t - 2r_0\sqrt{1-\left(\frac{R-t}{r_0}\right)^2} + 2(R-t)\cos^{-1}\left(\frac{R-t}{r_0}\right); & \text{for } r_0+t>R \text{ and } r_0-t\le R \\ 2\pi t - 2r_0\left(\sqrt{1-\left(\frac{R-t}{r_0}\right)^2} - \sqrt{1-\left(\frac{R+t}{r_0}\right)^2}\right); & \\ \quad +2(R-t)\cos^{-1}\left(\frac{R-t}{r_0}\right) - 2(R+t)\cos^{-1}\left(\frac{R+t}{r_0}\right); & \\ & \text{for } r_0-t\ge R. \end{cases} \tag{2}$$

Accordingly, the CDF of the distance to the nearest line of the BLP from a test point at $(0,r_0)$ is $F_d(t) = 1 - \mathcal{V}_{\mathrm{BLP}}(n_{\mathrm{B}},\mathcal{B}((0,r_0),t))$.

For further details on the properties of domain bands, please refer to [18].

B. Binomial Line Cox Process

If we define an independent 1D Poisson point process (PPP) Φ_i with intensity λ on each line L_i of $\mathcal{L}$, the collection of all such points on all lines of the BLP, i.e., $\Phi = \bigcup_{i=1}^{n_{\mathrm{B}}} \Phi_i$ is called the BLCP Φ.

Theorem 2. *The probability that the disk $\mathcal{B}((0,r_0),t)$ contains no points of Φ is given by*

$$\mathcal{V}_{\mathrm{BLCP}}(n_{\mathrm{B}},\mathcal{B}((0,r_0),t)) = \left[\frac{1}{2\pi R}\int_0^{2\pi}\int_{r_0\cos\theta-t}^{r_0\cos\theta+t} \exp\left(-\lambda C(\theta,r)\right)\,\mathrm{d}r\,\mathrm{d}\theta\right]^{n_{\mathrm{B}}}, \tag{3}$$

where

$$C(\theta,r) = \begin{cases} 2\sqrt{t^2-(r_0\cos\theta-r)^2}; & t\ge|r_0\cos\theta-r|, \\ 0; & \text{otherwise}, \end{cases} \tag{4}$$

is the length of the chord created by a line corresponding to $(\theta,r)\in\mathcal{D}$ in the disk $\mathcal{B}((0,r_0),t)$.

Corollary 1. *[Distance Distribution] Following the void probability, the distance distribution of the nearest BLCP point from the test point $(0,r_0)$ is*

$$F_{d_1}(t) = 1 - \mathcal{V}_{\mathrm{BLCP}}(n_{\mathrm{B}},\mathcal{B}((0,r_0),t)). \tag{5}$$

In the context of wireless networks, where APs are modeled as points in a BLCP, the outcome discussed above describes the distribution of distances to the nearest AP. We will leverage this to evaluate communication performance metrics in Section IV.

C. Line Length Density and Measure

The key motivation for studying BLP is to emulate distinct street densities in the city center and the suburbs. The *line length density* and *line length measure* are derived to characterize it.

Definition 1. *The line length measure is defined as*

$$\mathcal{R}(S) = n_{\mathrm{B}}\,\mathbb{E}\left(|L\cap S|_1\right),\ S\subset R^2,$$

where $|\cdot|_1$ is the Lebesgue measure in 1D and L is a line of the BLP. The corresponding radial density is

$$\rho(r) = \lim_{u\to 0}\frac{\mathcal{R}\big(\mathcal{B}((0,0),r+u)\setminus\mathcal{B}((0,0),r)\big)}{\pi(2u+u^2)}.$$

The line length measure follows by integrating $\rho(r)$, i.e., $\mathcal{R}(S) = \int_S \rho(|\mathbf{x}|)\,\mathrm{d}\mathbf{x},\quad S\subset\mathbb{R}^2$. In order to study the line length density, we first determine the expected total length of chords in a disk, i.e., its line length measure as defined above.

Theorem 3. *For a BLP generated by n_{B} lines within a disk of radius R,*

$$\rho(r) = \begin{cases} \frac{n_{\mathrm{B}}}{2R}, & \text{if } r\le R \\ \frac{n_{\mathrm{B}}}{\pi R}\arcsin\left(\frac{R}{r}\right) & \text{if } r>R. \end{cases}$$

Proof. Let $S = \mathcal{B}((0,r_0),t)$. We have

$$\mathcal{R}(S) = \mathbb{E}\left[K\bar{L}_1\right] = \bar{L}_1\mathbb{E}[K] \overset{(a)}{=} \bar{L}_1 n_{\mathrm{B}}\left(\frac{A_{\mathrm{D}}(r_0,t)}{2\pi R}\right), \tag{6}$$

where K is the number of lines intersecting disk $\mathcal{B}((0,r_0),t)$ and $\bar{L}_1$ is the expected length of the chord formed by a single line in the disk S. Step (a) follows from the expectation of the binomial distribution. For $\mathcal{B}((0,r_0),t)$, $\bar{L}_1$ is evaluated as

$$\bar{L}_1 = \frac{1}{A_{\mathrm{D}}(r_0,t)}\iint_{A_{\mathrm{D}}} 2\sqrt{(t^2-(r_0\cos\theta-r)^2)}\,\mathrm{d}r\mathrm{d}\theta,$$

where $A_{\mathrm{D}}(r_0,t)$ is obtained from (2).

Consider concentric circles centered at the origin having radii $l = \{w, 2w, \ldots\}$, where R is an integer multiple of

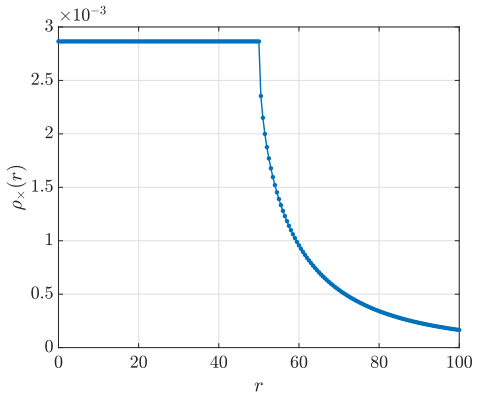

Fig. 1. Intersection density for $R = 50$ and $n_{\mathrm{B}} = 10$.

w. The annuli formed by these concentric circles have equal width w. Using (6), the ratio of the average length of line segments to the area in the $i-$th annulus, denoted by $\rho_i(w)$ is

$$\rho_i(w) = \begin{cases} \frac{n_{\mathrm{B}}}{2R}; & \text{for } (i+1)w \leq R, \\ \frac{n_{\mathrm{B}}}{\pi w^2(2i+1)} \Bigg(\sqrt{(i+1)^2w^2 - R^2} + \\ \left(\arcsin\left(\frac{R}{(i+1)w}\right) \times \frac{(i+1)^2w^2}{R}\right) - \sqrt{i^2w^2 - R^2} - \\ \left(\arcsin\left(\frac{R}{iw}\right) \times \frac{i^2w^2}{R}\right)\Bigg); & \text{for } (i+1)w > R. \end{cases} \tag{7}$$

Leveraging this, we can characterize the line length density of the BLP as a limiting function of the density in annuli. Precisely, the statement of the theorem is obtained by substituting $iw = r$ and taking the limit $w \to 0$ in (7). □

The density $\rho(r)$ remains constant at $\frac{n_{\mathrm{B}}}{2R}$ for $r \leq R$ and then decreases as $\mathcal{O}(1/r)$ as $r \to \infty$.

D. Intersection Density

Next, we characterize the point process formed by the intersections of the lines of the BLP.

Theorem 4. *The radial intersection density at a distance r from the origin for a BLP generated by n_{B} lines within a disk of radius R is*

$$\rho_\times(r) = \begin{cases} \frac{n_{\mathrm{B}}(n_{\mathrm{B}}-1)}{4\pi R^2}, & \text{if } r \leq R, \\ \frac{n_{\mathrm{B}}(n_{\mathrm{B}}-1)}{4\pi^2 R^2 r}\left(2r\arcsin\left(\frac{R}{r}\right) - \frac{2R}{r}\sqrt{r^2 - R^2}\right) & \text{if } r > R. \end{cases}$$

Proof. Please see Appendix A. □

In Fig 1 we see that intersection density first remains constant and then scales as $\mathcal{O}\left(\frac{1}{r}\right)$ as $r \to \infty$. By integrating the intersection density, we get the intersection measure

$$\mathcal{R}(S) = \int_S \rho_\times(|\mathbf{x}|)\, \mathrm{d}\mathbf{x}, \quad S \subset \mathbb{R}^2.$$

Remark 1. *The intersection measure of $\mathbb{R}^2$, as expected, is*

$$\mathcal{R}_\times = \int_0^{2\pi}\int_0^{\infty} \rho_\times(r)\, r\, \mathrm{d}r\, \mathrm{d}\theta = \binom{n_{\mathrm{B}}}{2} = \frac{n_{\mathrm{B}}(n_{\mathrm{B}}-1)}{2}.$$

III. Probability Generating Functional

A. A Palm Measure

Next, we study the BLCP from the perspective of a point of the process itself, using Palm calculus[2]. Let us recall that for a PLCP Φ_{PLCP} with λ as the density of the points on the lines, we have $\mathbb{P}(\Phi_{\mathrm{PLCP}} \in Y \mid o) = \mathbb{P}(\Phi_{\mathrm{PLCP}} \cup \Phi_0 \cup \{o\} \in Y)$, where Φ_0 is a 1D PPP on a line that passes through the origin. In other words, the Palm distribution, i.e., conditioning on a point of the PLCP Φ_{PLCP} to be at the origin, is equivalent to *adding* (i) an independent Poisson process of intensity λ on a line through the origin with uniform independent angle and (ii) an atom at the origin to the PLCP. Similarly, for a BLCP, conditioning on a point to be located at $\mathbf{x}$ is equivalent to considering an atom at $\mathbf{x}$, a 1D PPP on a line passing through $\mathbf{x}$ and a BLCP $\Phi^!$ defined on a BLP consisting of $n_{\mathrm{B}} - 1$ lines in the same domain. Thus, the Palm measure of the BLCP can be expressed as follows.

Lemma 1. *For a BLCP Φ defined on a BLP $\mathcal{P}$ with n_{B} lines, we have*

$$\mathbb{P}\left(\Phi \in Y \mid \mathbf{x} \in \Phi\right) = \mathbb{P}\left(\Phi^! \cup \Phi_{\mathbf{x}} \cup \{\mathbf{x}\} \in \mathbf{Y}\right), \tag{8}$$

where $\Phi_{\mathbf{x}}$ is a 1D PPP on a randomly oriented line that passes through $\mathbf{x}$.

The applications of the Palm measure will be evident in the next section where we analyze a wireless communication network. Prior to that, let us derive the PGFL of the shifted and reduced point process by conditioning on the location of the nearest point from the origin.

B. Probability generating functional of BLCP

Here, we characterize the PGFL of the BLCP Φ. In this paper, we are interested in isotropic functions that depend only on the distance of the points from the origin, i.e., we consider functions of the form $f(||\mathbf{x}||)$.

Definition 2. *Let $\mathbf{x}_1$ be the nearest point of a BLCP from $(0, r_0)$. Then, the shifted and reduced point process is defined as $\Phi' = \Phi - (0, r_0)\backslash\{\mathbf{x}_1\}$.*

The motivation for studying the properties of Φ' in the context of wireless networks is as follows; if the AP locations are modeled as a BLCP, then Φ' represents the locations of the interfering APs from the perspective of a user located at a distance r_0 from the origin and connected to an AP located at a distance $||\mathbf{x}_1||$ from the user. The next theorem characterizes the PGFL for the shifted and reduced BLCP Φ'.

Theorem 5. *For a shifted and reduced BLCP $\Phi' = \Phi - (0, r_0)\backslash\{\mathbf{x}_1\}$ defined on a BLP with n_{B} lines generated within $\mathcal{B}((0,0), R)$, the PGFL of a function $f(r) = f(||\mathbf{x}||)$, conditioned on $d_1 = ||\mathbf{x}_1||$ is given as*

$$G(r_0, f(\cdot)) = \frac{1}{A_{\mathrm{D}}(r_0, d_1)} \times$$

[2]In point process theory, the Palm probability refers to the probability measure conditioned on a point of the process being at a certain location [19].

$$\iint\limits_{\mathcal{D}_{\mathrm{B}}(0,d_1)} \exp\left(-2\lambda\int_{\sqrt{d_1^2-l^2}}^{\infty} 1-f\left(\sqrt{y^2+l^2}\right)\,\mathrm{d}y\right)\mathrm{d}r\mathrm{d}\theta\times$$
$$\left(\frac{1}{2\pi R}\right)^{n_{\mathrm{B}}-1}\left(\iint\limits_{\mathcal{D}_{\mathrm{B}}(0,d_1)} \exp\left(-2\lambda\int_{\sqrt{d_1^2-l^2}}^{\infty} 1-\right.\right.$$
$$\left.\left. f\left(\sqrt{y^2+l^2}\right)\,\mathrm{d}y\right)\mathrm{d}r\mathrm{d}\theta+\right.$$
$$\left.\iint\limits_{\mathcal{D}\setminus\mathcal{D}_{\mathrm{B}}(0,d_1)} \exp\left(-2\lambda\int_{0}^{\infty} 1-f\left(\sqrt{y^2+l^2}\right)\,\mathrm{d}y\right)\mathrm{d}r\mathrm{d}\theta\right)^{n_{\mathrm{B}}-1},$$

where $l = r_0\cos\theta - r$ and $d_1 = ||\mathbf{x}_1||$ is the distance to the nearest point of $\Phi-(0,r_0)$ from the origin. Consequently, the PGFL of Φ' is evaluated as $\mathbb{E}_{d_1}\left[G(r_0, f(\cdot))\right]$, where the distribution of d_1 is given by Corollary 1.

Proof. Please see Appendix B. □

IV. Application - Transmission Success Probability

In wireless networks, several performance metrics are studied using the *transmission success probability*. It is the complementary cumulative density function (CCDF) of the signal-to-interference-plus-noise ratio (SINR) over the fading coefficients and the spatial process of the locations of the APs. In this section, we define and characterize this metric using the results derived in the previous sections.

A. Success Probability - Definition

Let Φ be a point process containing points $\{\mathbf{x}_i\} \subset \mathbb{R}^2$, $i = 1, 2, \ldots$, and a test point at the origin, we can order the points of Φ according to their distance from the origin. The AP located at $\mathbf{x_1}$ is connected to the receiver at the origin, following the nearest-AP association. Small-scale fading takes place due to fluctuations of received power from multiple reflecting paths. Multiplying the received signal by a random variable h with exponential distribution with parameter 1 [20] accounts for the impact of small-scale fading. For a path-loss exponent α, the SINR $\xi(r_0)$ is

$$\xi(r_0) = \frac{\xi_0||\mathbf{x_1}||^{-\alpha}h_1}{1+\xi_0\sum_{\mathbf{x}\in\Phi\setminus\{\mathbf{x_1}\}}||\mathbf{x}||^{-\alpha}h_{\mathbf{x}}}, \tag{9}$$

where ξ_0 is a constant that takes into account the transmit power P, AWGN noise, path-loss constant, as well as the transmit and receive antenna gains. We assume that this parameter is the same for each transmit node. Typically, the $h_{\mathbf{x}}$ are independent of each other and identically distributed [20]. For the ease of notation, let us represent $||\mathbf{x_i}||$ by $d_{\mathbf{x}}$. Now, the transmission success probability at a threshold of γ is defined as the CCDF of $\xi(r_0)$ [20]:

$$p_{\mathrm{S}}(\gamma) = \mathbb{P}[\xi(r_0) > \gamma]. \tag{10}$$

This represents the probability that an attempted transmission by the nearest AP located at $\mathbf{x_1}$ is decoded successfully by the receiver at the origin. In what follows, we refer to the transmission success probability as *success probability*.

B. Success probability for BLCP Locations of APs

The BLCP model is useful for examining the placement of APs along city streets or industrial warehouses. The network's performance analysis depends on the location of the test point, but since the BLP is isotropic, it only depends on the distance from the center, not the orientation. We can assume the test point is on the x-axis and analyze the performance from the perspective of a point at $(0, r_0)$, without loss of generality. Equivalently, we can consider the receiver at the origin and study the statistics of the shifted point process $\Phi-(0,r_0)$. We assume the receiver connects to the nearest AP, experiencing interference from all other APs. In this case, the success probability is characterized as follows.

Theorem 6. *For the network where locations of the APs are modeled as BLCP, the success probability for a receiver located at $(0, r_0)$ is given by*

$$p_{\mathrm{S}}(\gamma) = \mathbb{E}_{d_1}\left[\exp\left(\frac{-\gamma}{\xi_0 {d_1}^{-\alpha}}\right) G\left(r_0, \frac{1}{1+\frac{\gamma r^{-\alpha}}{d_1^{-\alpha}}}\right)\right],$$

where $G(r_0, f(\cdot))$ is given by Theorem 5.

Proof. The success probability can be evaluated as

$$\begin{aligned} p_{\mathrm{S}}(\gamma) &= \mathbb{P}[\xi(r_0) > \gamma] = \mathbb{P}\left[\frac{\xi_0 {d_1}^{-\alpha}h_1}{1+\xi_0\sum_{\mathbf{x}\in\Phi'}{d_{\mathbf{x}}}^{-\alpha}h_{\mathbf{x}}} > \gamma\right] \\ &= \mathbb{P}\left[h_1 > \frac{\gamma\xi_0\sum_{\mathbf{x}\in\Phi'}{d_{\mathbf{x}}}^{-\alpha}h_{\mathbf{x}}+\gamma}{\xi_0 d_1^{-\alpha}}\right] \\ &= \mathbb{E}\left[\exp\left(\frac{-\gamma\xi_0\sum_{\mathbf{x}\in\Phi'}{d_{\mathbf{x}}}^{-\alpha}h_{\mathbf{x}}-\gamma}{\xi_0 d_1^{-\alpha}}\right)\right] \\ &= \mathbb{E}_{d_1}\left[\exp\left(\frac{-\gamma}{\xi_0 d_1^{-\alpha}}\right)\mathbb{E}^{!}_{\mathbf{x}_1,h_{\mathbf{x}}}\left[\exp\left(\frac{-\gamma\sum_{\mathbf{x}\in\Phi'}d_{\mathbf{x}}^{-\alpha}h_{\mathbf{x}}}{d_1^{-\alpha}}\right)\right]\right]. \end{aligned} \tag{11}$$

Here, $\mathbb{E}^{!}_{\mathbf{x}_1}$ refers to the expectation taken with respect to the Palm probability of the shifted and reduced point process, i.e., conditioned on a point of $\Phi-(0,r_0)$ being located at $\mathbf{x_1}$ and then removing it. The 1st term, $\exp\left(\frac{-\gamma}{\xi_0 d_1^{-\alpha}}\right)$, takes into account the impact of the noise and thus only depends on d_1 and N_0. The second term $\mathbb{E}^{!}_{\mathbf{x}_1,h_{\mathbf{x}}}[\cdot]$, takes into account the impact of the interference and can be further simplified

$$\begin{aligned} &\mathbb{E}^{!}_{\mathbf{x}_1,h_{\mathbf{x}}}\left[\exp\left(\frac{-\gamma\sum_{\mathbf{x}\in\Phi'}d_{\mathbf{x}}^{-\alpha}h_{\mathbf{x}}}{d_1^{-\alpha}}\right)\right] \\ &= \mathbb{E}^{!}_{\mathbf{x}_1}\left[\mathbb{E}_{h_1}\left[\prod_{\mathbf{x}\in\Phi'}\exp\left(\frac{-\gamma d_{\mathbf{x}}^{-\alpha}h_{\mathbf{x}}}{d_1^{-\alpha}}\right)\right]\right] \\ &= \mathbb{E}^{!}_{\mathbf{x}_1}\left[\prod_{\mathbf{x}\in\Phi'}\left[\mathbb{E}_{h_1}\exp\left(\frac{-\gamma d_{\mathbf{x}}^{-\alpha}h_{\mathbf{x}}}{d_1^{-\alpha}}\right)\right]\right] \\ &= \mathbb{E}^{!}_{\mathbf{x}_1}\left[\prod_{\mathbf{x}\in\Phi'}\frac{1}{1+\frac{\gamma d_{\mathbf{x}}^{-\alpha}}{d_1^{-\alpha}}}\right] = G\left(r_0, \frac{1}{1+\frac{\gamma r^{-\alpha}}{d_1^{-\alpha}}}\right) \end{aligned}$$

Applying the PGFL from Theorem 5 gives

$$G\left(r_0, \frac{1}{1+\frac{\gamma r^{-\alpha}}{d_1^{-\alpha}}}\right) = \frac{1}{A_{\mathrm{D}}(r_0,d_1)}\times$$
$$\iint\limits_{\mathcal{D}_{\mathrm{B}}(0,d_1)} \exp\left(-2\lambda\int_{\sqrt{d_1^2-l^2}}^{\infty}\left(\frac{\gamma\left[y^2+l^2\right]^{-\frac{\alpha}{2}}}{d_1^{-\alpha}+\gamma\left[y^2+l^2\right]^{-\frac{\alpha}{2}}}\right)\,\mathrm{d}y\right)\mathrm{d}r\mathrm{d}\theta$$

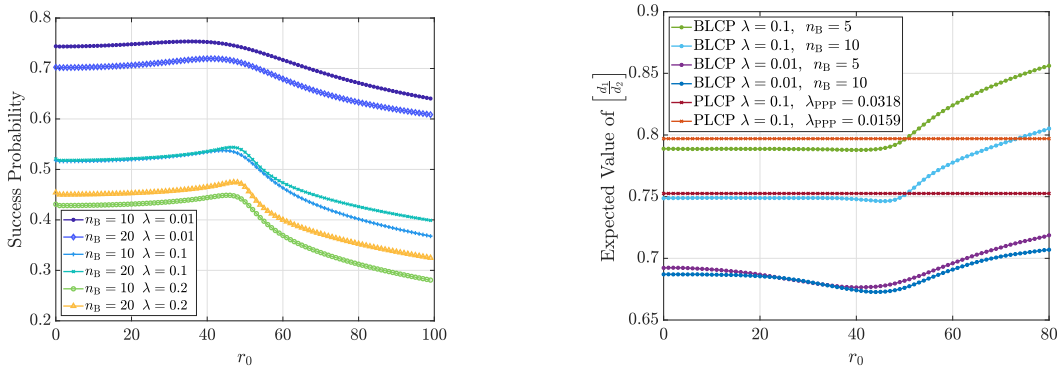

(a) (b)

Fig. 2. (a) Success probability with respect to r_0. Here $R = 50$. (b) $\mathbb{E}\left[\frac{d_1}{d_2}\right]$ with respect to r_0.

$$\left(\frac{1}{2\pi R}\right)^{n_B-1}\left(\iint_{\mathcal{D}_B(0,d_1)} \exp\left(-2\lambda\int_{\sqrt{d_1^2-l^2}}^{\infty}\left(\frac{\gamma\left[y^2+l^2\right]^{-\frac{\alpha}{2}}}{d_1^{-\alpha}+\gamma\left[y^2+l^2\right]^{-\frac{\alpha}{2}}}\right)\mathrm{d}y\right)\mathrm{d}r\mathrm{d}\theta+\iint_{\mathcal{D}\setminus\mathcal{D}_B(0,d_1)} \exp\left(-2\lambda\int_{0}^{\infty}\left(\frac{\gamma\left[y^2+l^2\right]^{-\frac{\alpha}{2}}}{d_1^{-\alpha}+\gamma\left[y^2+l^2\right]^{-\frac{\alpha}{2}}}\right)\mathrm{d}y\right)\mathrm{d}r\mathrm{d}\theta\right)^{n_B-1}.$$

Employing the above in (11) completes the proof. □

V. Numerical Results and Discussion

In this section, we discuss some numerical results to highlight the applications of the derived framework in analyzing the wireless network. Unless otherwise stated, all results are for $R = 50, \alpha = 2, \xi_0 = 2.9858 \cdot 10^{-8}$ and, $\gamma = 0.1$ dB.

A. On the Success Probability

In Fig. 2a, we plot the success probability with respect to r_0 for different values of λ and n_B. We observe that the success probability first increases slightly with r_0, reaches a maximum, and starts decreasing. To delve deeper into this phenomenon, we plot the expected value of the ratio of the distance from the nearest BLCP point to the distance of the second nearest BLCP point with respect to r_0 in Fig. 2b. In case the majority of the interference power is contributed by the nearest interferer, this parameter acts as a good indicator of the success probability. We note that the value of $\mathbb{E}\left[\frac{d_1}{d_2}\right]$ decreases with r_0 at first, reaches its minimum value near $r_0 = R$ and increases beyond that. This indicates that as we move away from the city center, although both the serving AP and the interferers become statistically distant from the test point, the relative increase in d_1 is higher as compared to the relative increase in d_2 with r_0. Such an insight for urban networks, in case the streets follow a BLCP cannot be obtained with PLCP models (also shown in Fig. 2b for different densities).

Next, consider a simple ALOHA access scheme where each interfering AP transmits with a probability p [21]. The success probability is obtained by weighting each interference term by the probability of the corresponding node transmitting. Fig. 3 plots the success probability w.r.t. location of AP for different values of λ, transmit power P, and transmission probability p. We see that for $P = 0.01$, and lower values of $\lambda \leq 0.01$ success probability decreases as r_0 goes from the city center to the outskirts irrespective of the value of p. However, for $\lambda \geq 0.05$, an optimum distance exists from the center where the success probability is maximum. The success probability for $\lambda = 0.001$ shows a varying trend for different transmit power values and transmission probability. When $P = 0.01$ and $p = 0$, $\lambda = 0.001$ results in the minimum success probability for all values of r_0. However, for $P = \{1, 10\}$ and $p = 1$, we observe the highest success probability for some initial values of r_0. The reason behind this is that a lower value of p leads to lower interference power. In this case, a lower density results in the serving AP being farther from the user, leading to poor success probability. Conversely, for a higher value of p, a lower value of λ proves beneficial to have fewer interferers near the user.

B. Optimal Network Parameters

In Fig. 4a-4c, we plot the success probability with respect to λ and n_B respectively for different values of r_0. We observe that an increase in the number of lines may increase or decrease the success probability depending on the location of the test device and the density of deployment. Particularly in Fig. 4a, a higher density of APs is favorable in a scenario with dense streets i.e. $n_B = 20$ as compared to $n_B = 10$. Thus, based on the location of the test device, there may exist an optimal deployment density of the APs. Fig. 4a shows that as λ increases the success probability decreases, due to the increase in interference, after a certain λ value, more streets provide a higher success probability than fewer streets. Similarly, in Fig. 4c, we observe that n_B maximizes the success probability for a given r_0 and λ. For high values of λ, the success probability increases with n_B and then decreases. Whereas the the success probability decreases with n_B for smaller values of λ. In Fig. 5 we plot the optimal value of λ versus the transmit power P for which the success probability is maximized for two different locations of test point i.e. $r_0 = 0$ and 200. We see that optimal λ decreases as P increases, indicating the relative reduction in deployment realizes an optimal success probability in the case of higher

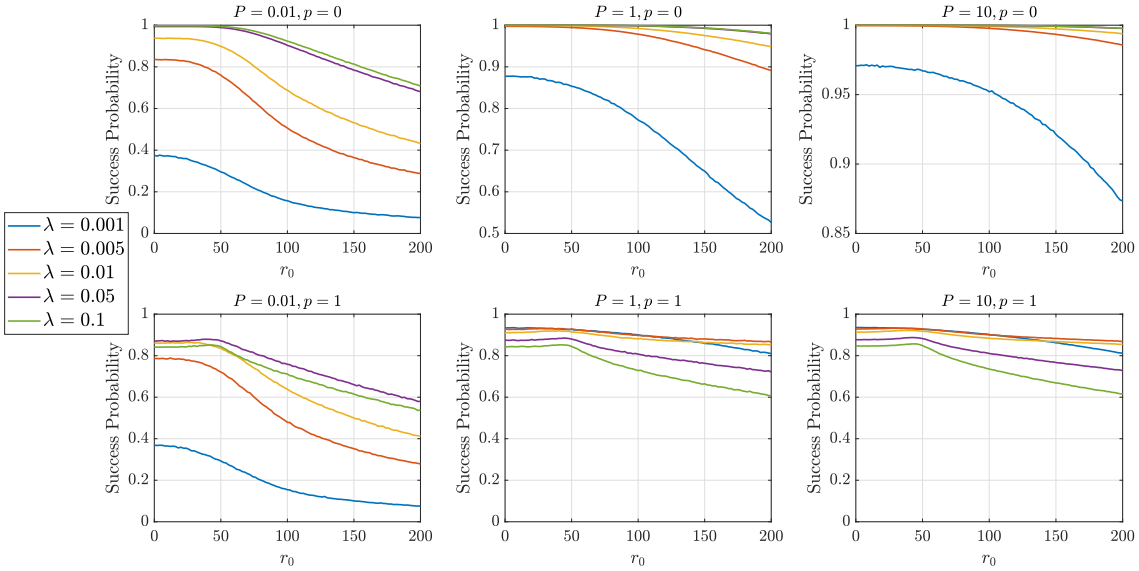

Fig. 3. Success probability for $\alpha = 4$ and different values of λ, power P and transmission probability p.

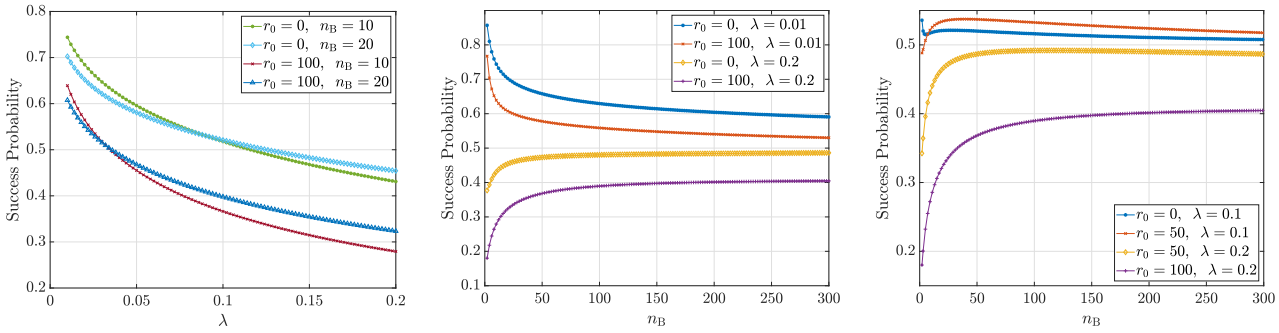

(a) (b) (c)

Fig. 4. (a) Success probability with respect to the density of APs. (b) & (c) Success probability with respect to n_{B}.

transmit powers. We also see that asymptotically optimal λ converges for $r_0 = 0$ and 200, thus indicating at higher P values, lower λ is desired regardless of whether the user is at the city center or outside the city.

VI. Conclusions and Future Work

We have characterized the binomial line Cox process (BLCP) which takes into account the non-homogeneity of lines in a Euclidean plane. Although there are several line processes studied in the literature, none of the existing models take into account the non-homogeneity of the lines. This is a drawback of the existing models since practical problems e.g., wireless network planning or transport infrastructure planning needs to deal with non-homogeneous streets in a city. We derive the line length density that help us visualize varying street densities. We also derive probability generating functional of the BLCP, and used it to analyze the transmission success probability in a wireless network. Then, we have provided extensive numerical results to derive system design insights for such network deployments. We envisage that the statistical model developed in this paper will be employed in the study of practical problems involving urban street planning. The shortest path length and non-homogeneous PLCP are indeed interesting directions of research, which will be taken up as future work.

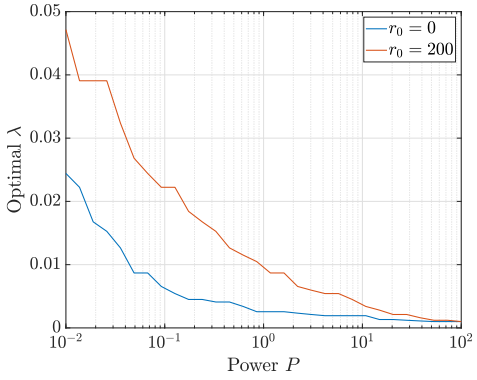

Fig. 5. Optimal λ versus transmit power. Note, here $\alpha = 4$.

References

[1] M. T. Shah, "Codes for BLP and BLCP: Statistical characterization and applications in wireless network analysis." Github, https://github.com/mt19146/blcp, 2023.

[2] M. T. Shah, G. Ghatak, S. Sanyal, and M. Haenggi, "Binomial line cox processes: Statistical characterization and applications in wireless network analysis," *arXiv preprint arXiv:2302.05151*, 2023.

[3] F. Baccelli *et al.*, "Stochastic geometry and architecture of communication networks," *Telecommunication Systems*, vol. 7, no. 1, pp. 209–227, 1997.

[4] H. S. Dhillon, R. K. Ganti, F. Baccelli, and J. G. Andrews, "Modeling and analysis of k-tier downlink heterogeneous cellular networks," *IEEE Journal on Selected Areas in Communications*, vol. 30, no. 3, pp. 550–560, 2012.

[5] H. ElSawy, E. Hossain, and M. Haenggi, "Stochastic geometry for modeling, analysis, and design of multi-tier and cognitive cellular wireless networks: A survey," *IEEE Communications Surveys & Tutorials*, vol. 15, no. 3, pp. 996–1019, 2013.
[6] G. Ghatak *et al.*, "Small cell deployment along roads: Coverage analysis and slice-aware RAT selection," *IEEE Transactions on Communications*, vol. 67, no. 8, pp. 5875–5891, 2019.
[7] V. V. Chetlur, *Stochastic Geometry for Vehicular Networks*. PhD thesis, Virginia Tech, 2020.
[8] B. Ripley, "The foundations of stochastic geometry," *The Annals of Probability*, vol. 4, no. 6, pp. 995–998, 1976.
[9] G. Mansfield, "Using Streetlights to Boost 5G Deployments in Cities," *https://about.att.com/innovationblog/2022/streetlights-to-boost-5g-deployments.html*, February 25, 2022.
[10] "NYC allows 5G equipment on streetlamps," *https://www.fiercewireless.com/5g/nyc-allows-5g-equipment-streetlamps*, 2020.
[11] W. S. Kendall, "From random lines to metric spaces," *The Annals of Probability*, vol. 45, no. 1, pp. 469–517, 2017.
[12] J. Kahn, "Improper Poisson line process as SIRSN in any dimension," *The Annals of Probability*, vol. 44, no. 4, pp. 2694–2725, 2016.
[13] J. P. Jeyaraj and M. Haenggi, "Cox models for vehicular networks: SIR performance and equivalence," *IEEE Transactions on Wireless Communications*, vol. 20, no. 1, pp. 171–185, 2020.
[14] N. Chenavier and R. Hemsley, "Extremes for the inradius in the Poisson line tessellation," *Advances in Applied Probability*, vol. 48, no. 2, pp. 544–573, 2016.
[15] V. V. Chetlur and H. S. Dhillon, "Coverage and rate analysis of downlink cellular vehicle-to-everything (C-V2X) communication," *IEEE Transactions on Wireless Communications*, vol. 19, no. 3, pp. 1738–1753, 2019.
[16] V. V. Chetlur and H. S. Dhillon, "On the load distribution of vehicular users modeled by a Poisson line Cox process," *IEEE Wireless Communications Letters*, vol. 9, no. 12, pp. 2121–2125, 2020.
[17] T. Courtat, C. Gloaguen, and S. Douady, "Mathematics and morphogenesis of cities: A geometrical approach," *Phys. Rev. E*, vol. 83, p. 036106, Mar 2011.
[18] G. Ghatak, "Binomial line processes: Distance distributions," *IEEE Transactions on Vehicular Technology*, vol. 71, no. 2, pp. 2176–2180, 2022.
[19] M. Haenggi, *Stochastic geometry for wireless networks*. Cambridge University Press, 2012.
[20] M. Haenggi *et al.*, "Stochastic geometry and random graphs for the analysis and design of wireless networks," *IEEE Journal on Selected Areas in Communications*, vol. 27, no. 7, pp. 1029–1046, 2009.
[21] N. Abramson, "The aloha system: Another alternative for computer communications," in *Proceedings of the November 17-19, 1970, Fall Joint Computer Conference*, AFIPS '70 (Fall), p. 281–285, Association for Computing Machinery, 1970.
[22] D. Stoyan, W. S. Kendall, S. N. Chiu, and J. Mecke, *Stochastic geometry and its applications*. John Wiley & Sons, 2013.

APPENDIX A
PROOF OF THEOREM 4

Consider a BLP line, L_0, that is generated at the point $(0, r_0)$ where $0 \leq r_0 \leq \min\{t, R\}$, ans let $S = \mathcal{B}((0,0), t)$. The domain band $\mathcal{D}_\times$ is determined by the intersection within S of L_0 and all $L_i \in \mathcal{L}$ lines. The range of r for a given θ where the generated line intersects $(0, r_0)$ within S is

$$\max\left\{-R, \left(r_0\cos\theta - \sqrt{t^2 - r_0^2}\sin\theta\right)\right\} \leq r_i \leq \min\left\{R, \left(r_0\cos\theta + \sqrt{t^2 - r_0^2}\sin\theta\right)\right\}.$$

For $t > R$, the domain band gets clipped to R and $-R$ in the upper and lower limits, thus the area of the domain band for these two cases i.e. $t \leq R$ and $t > R$ can be derived as follows.

Case 1: $t \leq R$. The domain band's area is averaged for uniformly distributed r_0 values between 0 and t. As $S \subset \mathcal{B}((0,0), R)$, there is no clipping in the values of r.

Case 2: $t > R$. Here $\mathcal{B}((0,0), R) \subset S$. Accordingly, the values of r are limited to R and $-R$. The values of θ for which r are clipped are obtained by solving for θ in the equations $r_0\cos\theta - \sqrt{t^2 - r_0^2}\sin\theta = -R$ and $r_0\cos\theta + \sqrt{t^2 - r_0^2}\sin\theta = R$, respectively. Thus, within these limits of θ, the area of the domain band for a line to intersect the line L_0 within S is

$$A_{D_\times}(t) = \begin{cases} \pi t; & \text{if } t \leq R, \\ \frac{2}{R}\Big(t^2 \arcsin\left(\frac{R}{t}\right) + \\ \quad 2R^2 \arccos\left(\frac{R}{t}\right) - \sqrt{t^2 - R^2}\Big); & \text{if } t > R. \end{cases}$$

Accordingly, the probability that a line intersects a single line within S is obtained as $\mathcal{P}_\times(t) = \frac{A_{D_\times}(t)}{2\pi\min\{t,R\}}$. Now, let us assume that k lines are generated in S. Each of these intersects L_0 with probability $\mathcal{P}_\times(t)$. As a result, the average number of intersections on L_0 within S from the k lines is

$$\mathcal{N}' = \sum_{j=0}^{k} j\binom{k}{j}\left(\mathcal{P}_\times(t \,|\, t \leq R)\right)^j \left(1 - \mathcal{P}_\times(t \,|\, t \leq R)^{k-j} = \frac{k}{2}.\right.$$

Finally in order to determine the average number of intersections on all the lines within S, we take the expectation over the number of lines are generated within S. This is evaluated as

$$\mathcal{N}_1 = \sum_{k=0}^{n_\mathrm{B}-1}\binom{n_\mathrm{B}}{k+1}\left(\frac{t}{R}\right)^{k+1}\left(1 - \frac{t}{R}\right)^{n_\mathrm{B}-k-1} \times \frac{k}{2} \times (k+1) \times \frac{1}{2} = \frac{n_\mathrm{B}(n_\mathrm{B}-1)}{4}\left(\frac{t}{R}\right)^2.$$

If $t > R$, n_B lines are generated, so the average number of intersections on all lines is determined similarly as

$$\mathcal{N}_2 = \sum_{k_1=0}^{n_\mathrm{B}-1} k_1 \mathcal{P}_\times(t \,|\, t > R) = \frac{n_\mathrm{B}(n_\mathrm{B}-1)}{2\pi R^2}\left(t^2 \arcsin\left(\frac{R}{t}\right) + R\left(2R\arccos\left(\frac{R}{t}\right) - \sqrt{t^2 - R^2}\right)\right).$$

Thus, the average number of intersections within a disk of radius t centered at the origin is

$$\mathcal{N} = \begin{cases} \frac{n_\mathrm{B}(n_\mathrm{B}-1)}{4}\left(\frac{t}{R}\right)^2; & \text{if } t \leq R, \\ \frac{n_\mathrm{B}(n_\mathrm{B}-1)}{2\pi R^2}\Big(t^2 \arcsin\left(\frac{R}{t}\right) + \\ \quad R\left(2R\arccos\left(\frac{R}{t}\right) - \sqrt{t^2 - R^2}\right)\Big); & \text{if } t > R. \end{cases} \tag{12}$$

Consider concentric circles centered at the origin with radii $l = \{w, 2w, \dots\}$. Equation (12) calculates the ratio of the average number of intersections to the area of $i-$th annulus which will help us to determine the intersection radial density.

$\rho_{\times,i}(w) =$

$$\begin{cases} \frac{1}{\pi w^2(2i+1)}\Big(\frac{n_{\rm B}(n_{\rm B}-1)}{4}\times \\ \qquad \Big(\frac{(w(i+1))^2}{R^2}-\frac{(wi)^2}{R^2}\Big)\Big); \quad \text{for } (i+1)w\le R, \\ \frac{n_{\rm B}(n_{\rm B}-1)}{2\pi^2R^2w^2(2i+1)}\Big((i+1)^2w^2\arcsin\Big(\frac{R}{(i+1)w}\Big)+ \\ \qquad 2R^2\arccos\Big(\frac{R}{(i+1)w}\Big)-R\sqrt{(i+1)^2w^2-R^2}- \\ \qquad i^2w^2\arcsin\big(\frac{R}{iw}\big)-2R^2\arccos\big(\frac{R}{iw}\big)+ \\ \qquad R\sqrt{i^2w^2-R^2}\Big); \qquad \text{for } (i+1)w>R. \end{cases}$$

The final result of the intersection radial density of a BLP can be obtained by substituting $iw = r$ and taking the limit $w \to 0$ in the equation above.

Appendix B
Proof of Theorem 5

Let $f(r)$ be a positive, measurable, monotonic, and bounded function for the first part of the proof. Here we will find the PGFL of the restricted point process $\Phi' \cap \mathcal{B}((0,0),t)$. The theorem follows from the monotone convergence theorem with $t \to \infty$. Recall that for a PPP of intensity λ and a function $\nu(\cdot)$, the PGFL is [22]:

$$G_{\rm PPP} = \exp\left(-\lambda \int_{\mathbb{R}^d} (1-\nu(\mathbf{x}))\,\mathrm{d}\mathbf{x}\right). \tag{13}$$

Next, note that the distance of a BLP line L_i corresponding to the generating point (r,θ) in $\mathcal{D}$ from the origin in $\mathbb{R}^2$ is $|r_0\cos\theta - r|$ and let $l = r_0\cos\theta - r$. A point located at a distance y from the perpendicular projection of $(0,r_0)$ to L_i, has a distance $\sqrt{y^2+l^2}$ from $(0,r_0)$. The length of the chord is $2\sqrt{t^2-l^2}$ when $t \ge |r_0\cos\theta - r|$.

$$\begin{aligned} &G_1(r_0,r,\theta) \\ &\quad = \lim_{t\to\infty} \exp\left(-2\lambda\int_0^{\sqrt{t^2-l^2}} 1-f\left(\sqrt{y^2+l^2}\right)\,dy\right) \\ &\quad \overset{(a)}{=} \exp\left(-2\lambda\int_0^{\infty} 1-f\left(\sqrt{y^2+l^2}\right)\,dy\right), \end{aligned}$$

where step (a) is due to the monotone convergence theorem. We can categorize each line in Φ' into two groups: (1) those that intersect with $\mathcal{B}((0,0),d_1)$ and (2) those that do not. For a particular r_0 and d_1, a line is intersecting if $|r_0\cos\theta - r| \ge d_1$ and non-intersecting otherwise. By averaging over $(r,\theta)\in\mathcal{D}$, we can express the PGFL of each group as

$$\begin{aligned} G_{\rm I}(r_0,d_1) &= \frac{1}{A_{\rm D}(r_0,d_1)}\times \\ &\iint\limits_{\mathcal{D}_{\rm B}(0,d_1)} \exp\left(-2\lambda\int_{\sqrt{d_1^2-l^2}}^{\infty} 1-f\left(\sqrt{y^2+l^2}\right)\,dy\right)\mathrm{d}r\mathrm{d}\theta, \\ G_{\rm NI}(r_0,d_1) &= \frac{1}{(2\pi R - A_{\rm D}(r_0,d_1))}\times \\ &\iint\limits_{\mathcal{D}\setminus\mathcal{D}_{\rm B}(0,d_1)} \exp\left(-2\lambda\int_{0}^{\infty} 1-f\left(\sqrt{y^2+l^2}\right)\,dy\right)\mathrm{d}r\mathrm{d}\theta. \end{aligned}$$

Next, note that the line containing the nearest point of the BLCP intersects the disk $\mathcal{B}((0,0),d_1)$ almost surely. Whereas, the other $n_{\rm B}-1$ lines may or may not intersect the disk. Thus, the PGFL for $\Phi - (0,r_0)$ is evaluated as

$$\begin{aligned} &G(r_0,f(\cdot)) \\ &\overset{(a)}{=} \underbrace{G_{\rm I}(r_0,d_1)}_{\rm T_1} \sum_{n=0}^{n_{\rm B}-1}\binom{n_{\rm B}-1}{n}\Bigg[\underbrace{\left(\frac{A_{\rm D}(r_0,d_1)}{2\pi R}\times G_{\rm I}(r_0,d_1)\right)^n}_{\rm T_2} \\ &\qquad \times \underbrace{\left(\left(1-\frac{A_{\rm D}(r_0,d_1)}{2\pi R}\right)\times G_{\rm NI}(r_0,d_1)\right)^{n_{\rm B}-n-1}}_{\rm T_3}\Bigg] \\ &\overset{(b)}{=} G_{\rm I}(r_0,d_1)\left(\frac{1}{2\pi R}\right)^{n_{\rm B}-1}\Big(A_{\rm D}(r_0,d_1)\,G_{\rm I}(r_0,d_1)+ \\ &\qquad (2\pi R - A_{\rm D}(r_0,d_1))\,G_{\rm NI}(r_0,d_1)\Big)^{n_{\rm B}-1}. \end{aligned}$$

In step (a), the term $\rm T_1$ corresponds to the line containing the nearest point. The term $\rm T_2$ corresponds to the probability that a set of n lines intersect the disk and the conditional PGFL given that the lines intersect the disk. The term $\rm T_3$ corresponds to the probability that a set of $n_{\rm B}-n-1$ lines do not intersect the disk and the conditional PGFL given that the lines do not intersect the disk. The statement of the theorem follows from the above.